

ON CLASSICAL FLUCTUATIONS OF BALLISTIC CONDUCTANCE

P.G. SILVESTROV

Instituut-Lorentz, Universiteit Leiden, P.O. Box 9506, 2300 RA Leiden, The Netherlands

Universal conductance fluctuations¹ in disordered systems are one of the most known quantum mesoscopic effects. For ballistic cavity with smooth confining potential however, one should observe a much larger classical sample-to-sample conductance fluctuations. It is shown, how bending of the phase space in case of chaotic dynamics leads to additional enhancement of such fluctuations.

1 Introduction

Recently a method for investigation of classical to quantum crossover in ballistic transport was proposed^{2,3}. It was expected to become an alternative of averaging over fictitious disorder used before⁴ in order to mimic the effect of classical chaos. One advantage of the method was a possibility of explicit accurate construction of solutions of the Schrödinger equation built from short classical trajectories (shorter than the Ehrenfest time $\tau_E \propto \ln \hbar$). A disadvantage was conjecturing the validity of Random Matrix Theory⁵ (RMT) to describe the effect of longer trajectories. Extensive numerical simulations were performed^{6,7} in order to verify the possibility of using RMT for only a part of phase space. Still the understanding of surprising accuracy of effective RMT remains a challenge. In this note however we make a step back and consider the pure classical contribution to sample-to-sample conductance fluctuations. These fluctuations, being \hbar^{-1} times larger⁷ than the famous universal conductance fluctuations¹, may be seen if by means of external gates one will change the chaotic dynamics in the cavity while keeping constant openings to 2DEG. In all existing analysis the chaos was taken into account via exponentially fast stretching and squeezing of areas in phase space. Here we go beyond this linear stretching approximation and show how anomalously large “fluctuations of the conductance fluctuations” appear due to bending of phase space.

2 Open billiard

Classical trajectories appear in a quantum mechanical scattering problem through the semiclassical wave function (for two spatial dimensions x, y and smooth confining potential $U(x, y)$)

$$\psi(x, y) = \sum_{\sigma} \sqrt{\rho_{\sigma}(x, y)} \exp[i\mathcal{S}_{\sigma}(x, y)/\hbar] . \quad (1)$$

Here the action \mathcal{S}_{σ} and density ρ_{σ} solve the Hamilton-Jacobi and continuity equations

$$|\nabla\mathcal{S}|^2 = 2m(E_F - U) , \quad \nabla \cdot (\rho\nabla\mathcal{S}) = 0. \quad (2)$$

The action is multivalued and the index σ labels the different sheets. A family of trajectories described by eqs. (2) forms a tube, as is shown in the figure 1, left. The requirement that ψ is single-valued imposes a quantization condition,

$$\oint p_y dy = (n + 1/2)h, \quad (3)$$

where the integral is taken over any contour enclosing the tube.

A complete description of the classical motion in the billiard is given by the surface of section shown in Fig. 1, right. The injected beam crosses the section for the first time over an

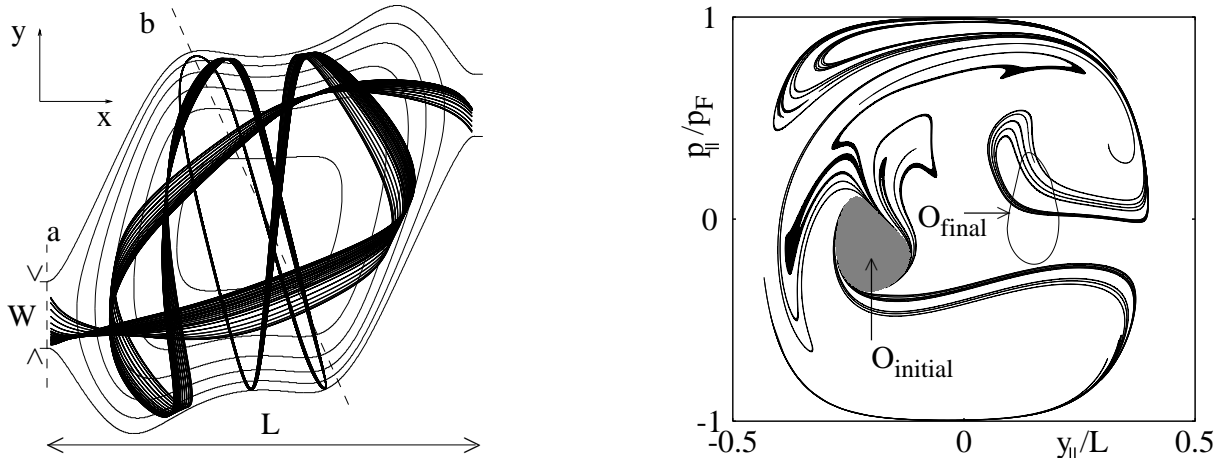


Figure 1: Left: Selected equipotentials of the electron billiard and a flux tube of transmitted trajectories representing the spatial extension of a fully transmitted scattering state. The outer equipotential defines the area which is classically accessible at the Fermi energy. The motion in the closed billiard is chaotic with Lyapunov exponent λ . Right: Section of phase space in the middle of the billiard (line b in left picture). Axes are the component of coordinate and momentum along this line. The area O_{initial} is the position of the first crossing of this surface of section by *all* possible at the Fermi energy injected trajectories. Elongated black areas O_j show the positions of the 5-th crossing of the injected beam with the surface of section. Points inside O_{final} leave the billiard without further crossing of line b .

area O_{initial} . Further crossings consist of increasingly more elongated ($\propto e^{\lambda t}$) areas O_j . The fifth crossing is shown in the figure. To leave the billiard (through the right contact) without further crossing of b a particle should pass through an area O_{final} . Consequently crossings of O_j with O_{final} indicate the trajectories leaving the billiard without further crossings with b and essentially without quantum interference. Following ref. ³ we will call these overlaps of O_j and O_{final} the transmission bands. Due to (3) the conductance is given by the sum of areas of intersection $G = \sum \oint \mathbf{p} \cdot d\mathbf{r}/h$. This counting of areas allows one to calculate the conductance as long as individual areas remains larger than h , which is the case for times shorter than τ_E . On the other hand, sample specific fluctuations of the biggest areas of intersection will lead to large, classical in essence, fluctuations of the conductance.

3 Quantum map model for ballistic cavity

Since the conductance is determined by the single surface of section we may investigate the general features of chaotic billiards by looking at the simple open map model ^{8,6,7}. An example of such map is given by the quantum kicked rotator ($p + 2\pi \equiv p, x + 2\pi \equiv x$)

$$H = \frac{\hat{p}^2}{2} + K \cos(x) \sum_n \delta(t - n), \quad \hat{p} = \frac{\hbar}{i} \frac{d}{dx}. \quad (4)$$

Choosing a special value of the Plank constant $\hbar \equiv 2\pi/M$ allows to work with a finite dimensional Hilbert space in both coordinate $x_k = k\hbar$, and momentum $p_m = m\hbar$ representations, $k, m = 1, 2, \dots, M$. This greatly simplifies the numerical calculation of the Floquet operator

$$U = e^{-i\hat{p}^2/2\hbar} e^{-iK \cos(x)/\hbar}. \quad (5)$$

The classical equations of motion for the kicked rotator are

$$\begin{cases} p_{n+1} = p_n + K \sin x_n \\ x_{n+1} = x_n + p_{n+1} \end{cases}. \quad (6)$$

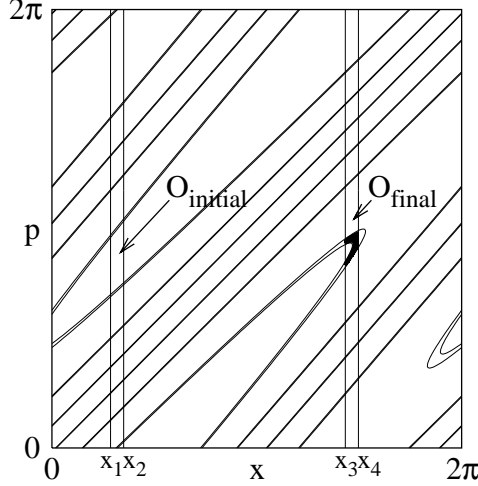


Figure 2: Second iteration of the map. Areas O_{initial} and O_{final} correspond to $x_1 < x < x_2$ and $x_3 < x < x_4$. Tilted narrow lines are the second image of the injected area O_{initial} . Their overlap with O_{initial} and O_{final} defines the transmission (reflection) bands. The black area shows the biggest transmission band.

The S -matrix for open kicked rotator is given by^{8,9}

$$S = P(1 - UQ)^{-1}UP^T = PUP^T + PUQUP^T + PUQUQUP^T + \dots \quad (7)$$

Here $Q = 1 - P^T P$, and a rectangular $2N \times M$ matrix P describes coupling to the leads. Two openings are placed at $x_1 < x < x_2$ (injected-reflected) and $x_3 < x < x_4$ (transmitted), where $x_2 - x_1 = x_4 - x_3 = w$. The only nonzero elements of the projection matrix P are $P_{i, i+I_{in}} = P_{i+N, i+I_{out}} \equiv 1$, where $I_{in} = Mx_1/2\pi$, $I_{out} = Mx_3/2\pi$ and $0 < i \leq N$.

The dimensionless conductance follows from the Landauer formula $G = \text{Tr}T$, where the transmission matrix $T = t^+ t$ is determined by the upper-right $N \times N$ sub-block t of the S -matrix. In our classical limit however calculation of the trace of transmission matrix reduces to the simple counting of areas of intersections in the x, p plane.

4 Sample specific conductance fluctuations

For kicked rotator (4) the developed chaos corresponds effectively to $K \gg 1$ (the Lyapunov exponent is $\lambda \approx \ln(K/2)$). Therefore the calculation in this section will be done in the leading order in $1/K$. Assuming the ergodic motion we may find the averaged number of transmitted or reflected channels at the n -th iteration of the map

$$\overline{T}_n = \overline{R}_n = \frac{Nw}{2\pi} \exp[-(n-1)w/\pi] \quad (8)$$

We are now interested in the fluctuations of these numbers caused by the variations in the leads position. The fluctuations are naturally more pronounced for small n . In our particular example however the first iteration $n = 1$ turns out to be trivial. The image of initially injected beam of particles after one iteration covers the area between two parallel lines $p + x_1 < x < p + x_2$. The numbers of transmitted and reflected channels are given by the eq. (8) and do not fluctuate.

Sample specific fluctuations of conductance first appear at the second iteration, as is illustrated by Fig 2. The typical number of channels in the transmission band is of the order of $\sim Nw/K$. However, if the lead will be placed close to one of the turning points of the bent image of the opening, the number may become as large as $N\sqrt{w/K}$. For narrow openings $w \ll 1$ and $K \gg 1$, these largest transmission bands cover an area between two inclined parabolas,

$$p = x \pm \sqrt{2x/K} \quad \text{and} \quad p = x \pm \sqrt{2(x-w)/K} \quad (9)$$

A simple integration allows to find the areas of intersection for different relative positions of the openings. This results in a probability distribution for large numbers of transmitted channels

$$P(T_2) = \frac{4N^2 w^2}{\pi^3 K T_2^3}, \quad \text{where } \frac{Nw}{\sqrt{K}} < T_2 < \frac{N\sqrt{w}}{K}. \quad (10)$$

The same probability distribution describes fluctuations of the number of reflected channels R_2 .

Contributions to conductance coming from the transmission bands which appear at the third and higher iterations of the map contain extra factors K^{-1} and their fluctuations may be neglected. Thus the dimensionless conductance has a form $G = T_2 + (N - T_2 - R_2)/2$ and the fluctuation of conductance is $\delta G \approx T_2/2 - R_2/2$. The power law tail of distribution (10) leads to the additional $\sim \ln(w)$ enhancement of the second moment

$$\langle \delta G^2 \rangle = \frac{w^2 N^2}{K \pi^3} \ln\left(\frac{1}{w}\right). \quad (11)$$

This logarithmic dependence on w ($w \ll 1$) may be responsible for the deviations from the scaling $\langle \delta G^2 \rangle \sim w^2 N^2$ observed in numerical simulations⁷.

Numerical coefficients in eqs. (10,11) are specific for the model (4,7). In more realistic case of a ballistic quantum dot of the size L coupled to the leads by two N -mode contacts eqs. (10,11) transform into

$$P(\delta G) \sim \frac{N^4}{(k_F L)^2} \frac{1}{\delta G^3}, \quad \langle \delta G^2 \rangle \sim \frac{N^4}{(k_F L)^2} \ln\left(\frac{k_F L}{N}\right). \quad (12)$$

Several experiments^{10,11} were performed recently aimed to observe quantum to classical crossover in quantum dots. In the experiment of this kind one is able to vary manually the conductance of the contacts and the shape of the dot. Further improvement of this technic may lead to experimental verification of our results.

Acknowledgments

Discussions with C.W.J. Beenakker and J. Tworzydło are greatly appreciated. This work was supported by the Dutch Science Foundation NWO/FOM.

References

1. B.L. Altshuler, JETP Lett. **41**, 648 (1985); P.A. Lee and A.D. Stone, Phys. Rev. Lett. **55**, 1622 (1985).
2. P.G. Silvestrov, M.C. Goorden, and C.W.J. Beenakker, Phys. Rev. Lett. **90**, 116801 (2003).
3. P.G. Silvestrov, M.C. Goorden, and C.W.J. Beenakker, Phys. Rev. B **67**, 241301 (2003).
4. I.L. Aleiner and A.I. Larkin, Phys. Rev. B **54**, 14423 (1996).
5. C.W.J. Beenakker, Rev. Mod. Phys. **69**, 731 (1997).
6. Ph. Jacquod, H. Schomerus, and C.W.J. Beenakker, Phys. Rev. Lett. **90**, 207004 (2003); M.C. Goorden, Ph. Jacquod, and C.W.J. Beenakker, Phys. Rev. B **68**, 220501 (2003); J. Tworzydło, A. Tajic, H. Schomerus, and C.W.J. Beenakker, Phys. Rev. B **68**, 115313 (2003); A. Kormanyos, Z. Kaufmann, C.J. Lambert, J. Cserti, cond-mat/0309306.
7. J. Tworzydło, A. Tajic, and C.W.J. Beenakker, Phys. Rev. B **69**, 165318 (2004); Ph. Jacquod and E.V. Sukhorukov, Phys. Rev. Lett. **92**, 116801 (2004).
8. A. Ossipov, T. Kottos, and T. Geisel, Europhys. Lett. **62**, 719 (2003).
9. Y.V. Fyodorov and H.-J. Sommers, JETP Lett. **72**, 422 (2000).
10. S. Oberholzer, E.V. Sukhorukov, and C. Schönberger, Nature **415**, 765 (2002).
11. R. Crook, C.G. Smith, A.C. Graham, I. Farrer, H.E. Beere, D.A. Ritchie Phys. Rev. Lett. **91**, 246803 (2003)